

Full paper

Colloidal thick-shell pyramidal quantum dots for efficient hydrogen production



Haiguang Zhao^a, Guiju Liu^a, François Vidal^{b,*}, Yiqian Wang^{a,*}, Alberto Vomiero^{c,*}

^a State Key Laboratory & College of Physics, Qingdao University, No. 308, Ningxia Road, Qingdao 266071, PR China

^b Énergie Matériaux Télécommunications, Institut National de la Recherche Scientifique, Québec University, 1650 Boulevard Lionel-Boulet, Varennes, Québec J3X 1S2, Canada

^c Division of Materials Science, Department of Engineering Sciences and Mathematics, Luleå University of Technology, 971 87 Luleå, Sweden

ARTICLE INFO

Keywords:

Pyramidal structure
Quantum dots
Water splitting
Core/thick-shell
Hydrogen generation

ABSTRACT

Colloidal semiconductor quantum dots (QDs) have attracted a great attention for their potential applications in optoelectronic devices, such as water splitting, luminescent solar concentrators, and solar cells, because of their size/shape/composition-dependent optoelectronic properties. However, the fast electron-hole (e-h) recombination and slow charge separation of QDs limit their applications as light absorbers in high-efficiency optoelectronic devices. Here, we synthesized thick-shell CdSe/CdSe_xS_{1-x}/CdS QDs with pyramidal shape, which exhibit a quantum yield of ~15%, with a long radiative lifetime up to ~100 ns due to the spatial separation of the e/h wavefunction and significantly broadened light absorption toward the 500–700 nm range, compared to CdSe/CdS unalloyed QDs. As a proof-of-concept, the pyramidal QDs are applied as light absorbers in a photoelectrochemical (PEC) system, leading to a saturated photocurrent density of ~12 mA/cm² (with a H₂ generation rate of 90 mL cm⁻² day⁻¹), which is a record for thick-shell QD-based photoelectrodes in PEC hydrogen generation. Core/thick-shell QDs hold great potential for breakthrough developments in the field of QD-based optoelectronic devices.

1. Introduction

The conversion of solar energy into electrical/chemical energy is one of the most efficient ways to solve the current challenges in the growing global demand for clean energy and the decreasing carbon dioxide emission [1,2]. The photoelectrochemical (PEC) water splitting is a promising solution to address these challenges because PEC devices can directly convert water into hydrogen (H₂) using solar energy as the primary energy source [3–6]. Usually, an ideal PEC cell is composed of safe and cost-effective semiconductor materials with suitable electronic band structure for efficient water reduction, wide sunlight absorption spectrum and high photochemical stability. Due to the wide band gap energy of the conventional metal oxide semiconductors (e.g. TiO₂, ZnO, SnO₂), these semiconductors can only absorb solar energy in the ultraviolet (UV) range [3–5,7]. Recent research is still focusing on the improvement of solar absorption by H-doping of metal oxides, the growth of metal oxides by atomic layer deposition, tailoring the surface states of metal oxides by post-surface treatments, etc [8–12]. Due to the limited light absorption of metal oxides, it is still very challenging to fabricate PEC devices with large H₂ production rate.

Recently colloidal semiconductor quantum dots (QDs) have attracted great attention for their potential applications as building blocks in optoelectronic devices, such as PEC water splitting, luminescent solar concentrators, light emitting devices, and solar cells, because of their size/shape/composition-tuneable wide absorption spectrum (ranging from UV to near infrared region), high absorption coefficient and cost-effective synthetic approaches [7,13–20]. Moreover, the bandgap structure of QDs can be easily tuned by controlling their structure and surface capping ligands, [18,19,21–27] which allows us to improve their charge dynamics, and thus solar-to-H₂ conversion efficiency in optoelectronic devices. Colloidal QDs have been applied to sensitize large band gap TiO₂ in PEC cells in order to improve the light absorption [7,13,28,29]. For examples, various types of QDs, including plain QDs (e.g. CdSe, PbS), alloyed QDs (CuInSeS), core/thin-shell QDs (e.g. PbS/CdS, CuInSeS/ZnS), and core/thick-shell QDs (e.g. CdSe/CdS, CuInSe/CuInS) have been shown to be effective sensitizers in PEC cells with saturated photocurrent densities in the range of 2–15 mA/cm² (Table S1) [7,13,28,29]. However, the solar-to-H₂ conversion efficiency obtained so far in PEC cells based on colloidal QDs is still low because of the limited absorption of QDs, inefficient electron-hole (e-h) pair

* Corresponding authors.

E-mail addresses: Vidal@emt.inrs.ca (F. Vidal), yqwang@qdu.edu.cn (Y. Wang), alberto.vomiero@ltu.se (A. Vomiero).

<https://doi.org/10.1016/j.nanoen.2018.08.042>

Received 29 May 2018; Received in revised form 7 August 2018; Accepted 19 August 2018

Available online 22 August 2018

2211-2855/ © 2018 Elsevier Ltd. All rights reserved.

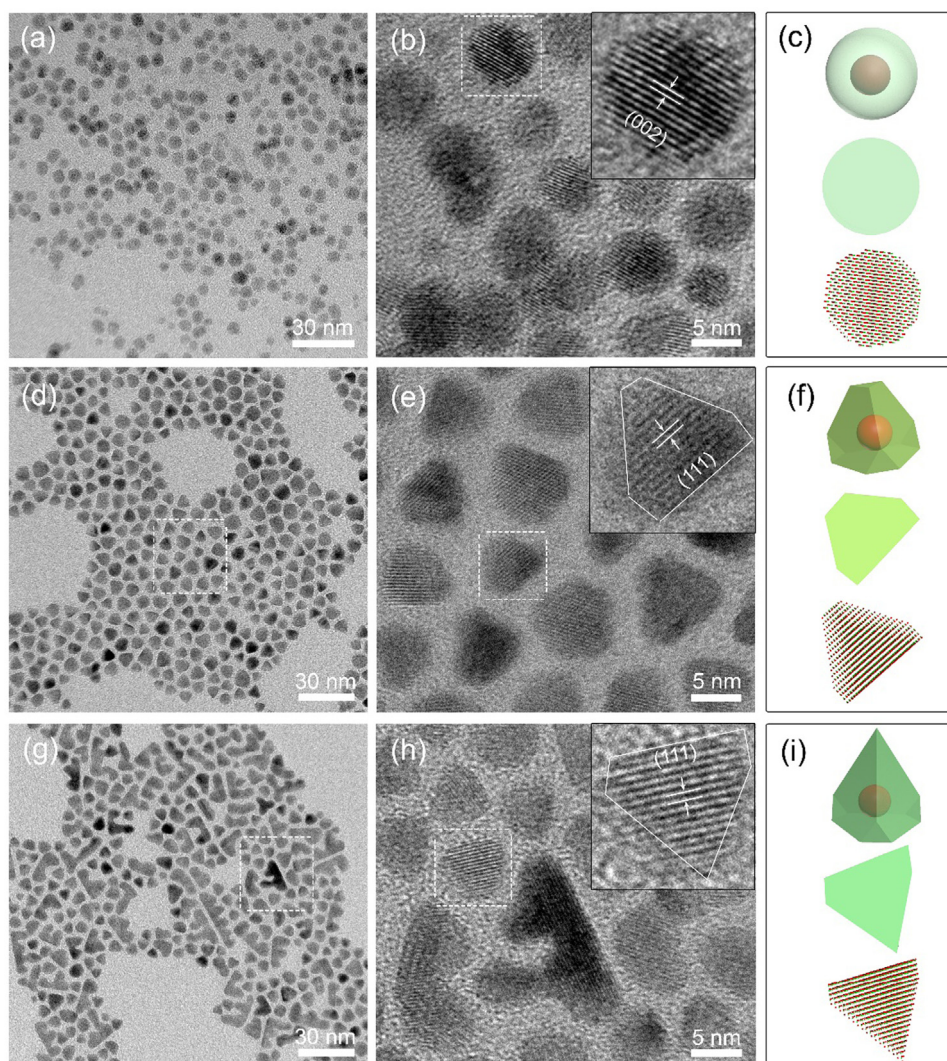


Fig. 1. Morphological and structural characterizations of core/thick-shell QDs. TEM and HRTEM images of CdSe/6CdS QDs with the shell growth at 240 °C (a, b) and 200 °C (d, e). (g, h) TEM and HRTEM images of CdSe/5CdSe_{0.5}S_{0.5}/CdS QDs with the shell growth at 200 °C. The insets in b, e and h are the corresponding HRTEM images of a single QD. (c, f and i) The 3D geometric models, 2D geometric projections and atomic models in a certain viewing direction of spherical CdSe/6CdS QDs, truncated pyramidal CdSe/6CdS QDs and CdSe/5CdSe_{0.5}S_{0.5}/CdS QDs.

generation/separation, and slow charge transport rate in presence of charge scavengers. Compared with the fast exciton recombination in spherical shape QDs, [20,23,30] recently, core/shell QDs (e.g. pyramidal, bipyramidal, tetrapoidal, dot-in-plate and dot-in-rod) [31–36] have been shown to exhibit not only efficient e-h pair separation due to the spatial distribution of the e-h pair, but also efficient charge transfer for both electrons and holes in presence of e/h scavengers. The electron transfer rate of the thick-shell CdSe/CdS QDs in mesoporous TiO₂ (shell thickness over 2 nm) can be largely improved compared with plain or core/thin-shell QDs due to the formation of quasi-type II band structure (in which electrons partially leak into the thick shell, but the holes are still confined in the core region [7]. In the thick-shell QDs systems (also called “giant” QDs), [21,27,34,37] the thick-shell slows down the hole transfer, leading to strong hole accumulation [7,13,28,29]. Usually, the hole accumulation leads to the strong surface oxidation of QDs, increasing the number of surface recombination centers or the degradation of QDs under illumination [7,13]. As a result, the thick-shell leads to the decrease in solar-to-H₂ conversion efficiency in QD-based PEC cells because of the self-oxidation, even the electron still can efficiently transfer to the electron acceptors (such as metal oxide) [7,13]. In the dot-in-rod CdSe/CdS system, [36] the CdS shell around CdSe core is less than 1 nm, which still allows efficient hole transfer. Meanwhile, the

electron can leak into the rod, forming a quasi-type II band structure to enhance the electron transfer rate. Unfortunately, these dot-in-rod QDs generally have a long length (> 20 nm), [36] making it technically difficult for their deposition into mesoporous TiO₂ thin films, which are typically used as QD scaffolds and electron acceptors in PEC cells [5]. To the best of our knowledge, there is only one report using pyramidal core/thin-shell CuInSSe/ZnS QDs for high-efficient PEC hydrogen generation with the highest saturated photocurrent density (J) of $\sim 5.3 \text{ mA/cm}^2$ [29]. Current research efforts are still focusing on the improvement of the efficiency of PEC devices by i) enhancing the light harvesting range of QDs; ii) improving the charge separation/transfer efficiency by designing heterostructure QDs; iii) enhancing the long-term chemical-/photo- stability of PEC devices by using core/thick-shell QDs as light absorbers.

Here, we synthesized pyramidal thick-shell CdSe/CdSe_xS_{1-x}/CdS QDs by controlling the reaction temperature and the molar ratio of Se/S precursors. The as-obtained CdSe/CdSe_xS_{1-x}/CdS QDs have an absorption spectrum from 300 to 670 nm, covering the UV and almost whole visible range, which is much wider than that of CdSe/CdS QDs with pyramidal or spherical shape (< 500 nm). Lifetime measurement and theoretical simulations of the e/h wave function as a function of geometry and chemical composition show that pyramidal thick-shell QDs

exhibit efficient e/h leakage to the shell range, but slightly increase the overlap of e/h wave function compared with spherical CdSe/CdS QDs with similar shell thickness. As a proof-of-concept, we used the thick-shell pyramidal QDs as photosensitizers for PEC H_2 generation. We obtained a saturated J as high as $\sim 12 \text{ mA/cm}^2$, nearly 1.7 and 1.3 times higher than the values obtained from spherical CdSe/CdS and pyramidal CdSe/CdS QDs, respectively, under identical preparation and measurement conditions. This value is a record for PEC devices based on thick-shell “giant” QDs. Our results indicate that pyramidal thick-shell heterostructured CdSe/CdSe $_x$ S $_{1-x}$ /CdS QDs can serve as efficient photosensitizer for optoelectronic devices, such as PEC H_2 generation or QDs sensitized solar cells.

2. Results and discussion

2.1. Synthesis of pyramidal core/thick-shell QDs

We first synthesized CdSe QDs via a hot injection approach [7,38]. Then the as-obtained CdSe QDs with a core diameter of 3.3 nm were used as seed for the synthesis of core/shell QDs via a successive ionic layer adsorption reaction (SILAR) (Fig. S1) [7,38]. Similar to reported results in the literature, [7,21,35,37–39] at the reaction temperature of 240 °C, a typical spherical shape of core/thick-shell QDs (CdSe/CdS) was obtained (Fig. 1a,b) and the diameter of the as-synthesized QDs is $(7.2 \pm 0.5) \text{ nm}$ with a shell thickness of around 2 nm after the growth of 6-monolayer CdS. As reported in the literature, typical core/shell structures have been proved as the overall size of QDs gradually increase with the increase of the growth cycles of the shell. However, due to the small lattice mismatch of CdSe core and CdS shell ($< 4.2\%$), it is still very challenging to directly observe the core/shell structure in CdSe/CdS QDs [19,21,35,37,40,41]. From the x-ray diffraction (XRD) patterns (Fig. S2), it can be seen that the structure of the CdSe core QDs is zinc blende (ZB), while the CdSe/CdS QDs synthesized at 240 °C shows the wurtzite (WZ) crystal structure which can be further confirmed by the selected-area electron diffraction (SAED) patterns in Fig. S3(a). Based on the high-resolution transmission electron microscopy (HRTEM) image (inset in Fig. 1b), the calculated lattice spacing of the spherical-shape CdSe/6CdS QD is 3.31 Å corresponding to the (002) plane of WZ crystal structure of CdS. In a big contrast, the QDs with quasi-pyramidal shapes were obtained by setting the reaction temperature at 200 °C during the growth of 6-monolayer CdS shell (Fig. 1d,e and Fig. S4a), and the structure of the QDs maintains the ZB phase of the core QDs (Figs. S2, S3b). All other reaction parameters (such as the concentration of seed QDs, the molar ratio of QDs to precursors, reaction time and concentration of precursors) are identical: the different shapes of QDs are mainly due to the different growth temperatures of the CdS shell during the SILAR process. Similar temperature-dependent morphologies of core/shell QDs were reported in PbSe/CdSe/CdS QDs, [27,32] in which QDs with spherical, pyramidal and tetragonal shapes were obtained by setting the CdS shell growth temperature at 240 °C, 200 °C, and 170 °C, respectively. Usually, the shell growth temperature-dependent morphologies of core/shell QDs are attributed to the kinetics of Cd and S atom deposition, where reduced temperatures were believed to induce delayed growth and, subsequently, higher precursor supersaturation followed by fast growth of certain facets [27,32]. Other factors (e.g. core crystalline structure and the influence of ligands) [22,31,34,35] were also found to affect the geometry of the core/shell QDs. As the surfactant and core seed used in this study are the same for spherical and pyramidal QDs, their role in determining the different morphologies in CdSe/CdS QDs can be ruled out. The CdSe QDs have a typical ZB crystal structure as reported in the literature using the same synthetic approach and recipe [7,38]. When the core CdSe QDs are covered with a CdS shell under 200 °C, the structure of the shell layer tends to maintain the crystal structure of the core QDs, which was demonstrated by the XRD patterns in Fig. S2. The SAED patterns of pyramidal-shape CdSe/CdS QDs (Fig. S3b) further

confirmed the ZB phase of CdS. From the XRD patterns of CdSe/CdS QDs (red line) in Fig. S2, it can be seen that the CdS shell and CdSe core have a certain epitaxially relationship, demonstrating that the CdS shell layer is epitaxially grown on planes of the CdSe core. With reaction time was prolonged, the morphologies of the QD were gradually transformed into a triangular pyramid consisting of 4 equivalent {111} planes. Transmission electron microscopy (TEM) measurements display the existence of different two-dimensional (2D) particle outlines under different projections. The majority of the QDs display a truncated-triangular outline. Considering the different 2D outlines from different projections of the QDs and the epitaxial growth of CdS shell, the 3D particle shape of a truncated triangular pyramid was proposed, as shown in Fig. 1f. The typical truncated-triangular and polygon outlines and their corresponding geometric model projections and atomic model projections are shown in Fig. 1e,f and Fig. S5. For the truncated-triangular (inset in Fig. 1e and Fig. S5a), the lattice spacing of the fringes was measured to be $\sim 3.39 \text{ \AA}$, corresponding to that of the {111} planes of ZB CdS. When viewed along the [011] zone axis (Fig. S5b), the lattice spacings of 3.36 Å and 3.08 Å were measured, which are associated with the ($\bar{1}\bar{1}\bar{1}$) and (200) planes, respectively. These results are consistent with the proposed geometric and atomic models, proving that the proposed models are correct.

We further synthesized core/alloyed shell QDs with the growth of 5 interfacial layers of CdSe $_x$ S $_{1-x}$ ($x = 0.5$) and 1 monolayer of CdS at 200 °C (denoted as CdSe/5CdSe $_{0.5}$ S $_{0.5}$ /CdS) (details in Section 4). As shown in Fig. 1g, most of the as-obtained CdSe/5CdSe $_{0.5}$ S $_{0.5}$ /CdS QDs have a pyramidal shape, which is very different from the spherical shape of the CdSe/5CdSe $_{0.5}$ S $_{0.5}$ /CdS QDs synthesized at 240 °C using the SILAR approach. [41] Similar to Fig. 1d, most of the QDs seen in the TEM images show a partially-truncated triangle. The model was generated by cutting the ZB CdS crystal into a truncated pyramid shape with 7 equivalent {111} planes merging into one apex (Fig. 1i). The shape, lattice fringes, as well as the measured lattice spacing, can all be matched to the geometric and atomic models. Based on the TEM measurement, the CdSe/5CdSe $_{0.5}$ S $_{0.5}$ /CdS QDs have a final diameter of $(8.1 \pm 0.7) \text{ nm}$ (the size of these QDs is defined as the height of the projected triangles), very similar to that of truncated-pyramidal CdSe/CdS QDs (Fig. S4a and Fig. 1d). From the projection, the thickness was estimated to be 2.65 nm and 5.35 nm from the center of CdSe QDs to the face center and corner of core/shell QDs, respectively. HRTEM analysis confirms the lattice parameters of the ZB structure in CdSe/5CdSe $_{0.5}$ S $_{0.5}$ /CdS QDs (Fig. 1h), consistent with the SAED patterns (Fig. S3c). The lattice spacing of pyramidal-shape CdSe/5CdSe $_{0.5}$ S $_{0.5}$ /CdS QDs is measured to be 3.48 Å which corresponds to the {111} planes of the ZB crystal structure of the studied QDs (inset in Fig. 1h). X-ray energy dispersive spectroscopy (EDS) and x-ray photoelectron spectroscopy (XPS) spectra of CdSe/CdS and CdSe/5CdSe $_{0.5}$ S $_{0.5}$ /CdS QDs confirm the presence of Cd, Se and S in the QDs with Se/S molar ratio of around 1 (Figs. S6–7).

As the obtained CdS or CdSeS shell thickness is between 2.65 nm and 5.35, i.e. thicker than 2 nm, and the optical properties of the core/shell QDs still exhibit strong quantum confinement, we named the currently obtained core/shell QDs as “giant” QDs, according to the literature [2,21,42]. In addition, our giant pyramidal core/shell QDs are different from the previously reported pyramidal bare CdSe QDs with a WZ structure [43].

2.2. Optical properties of the QDs

The first-excitonic absorption and emission peaks of pure CdSe QDs are around 550 nm and 560 nm, respectively (Fig. 2a,b). Further CdS coating via a SILAR method leads to strong absorption in the visible range (less than 500 nm) due to the large CdS shell volume content (92%) in the spherical and pyramidal shape CdSe/CdS QDs (Fig. 2a). Again, due to the large CdS shell volume, in the core/shell CdSe/CdS QDs (spherical or pyramidal), the absorption of CdSe core in the range

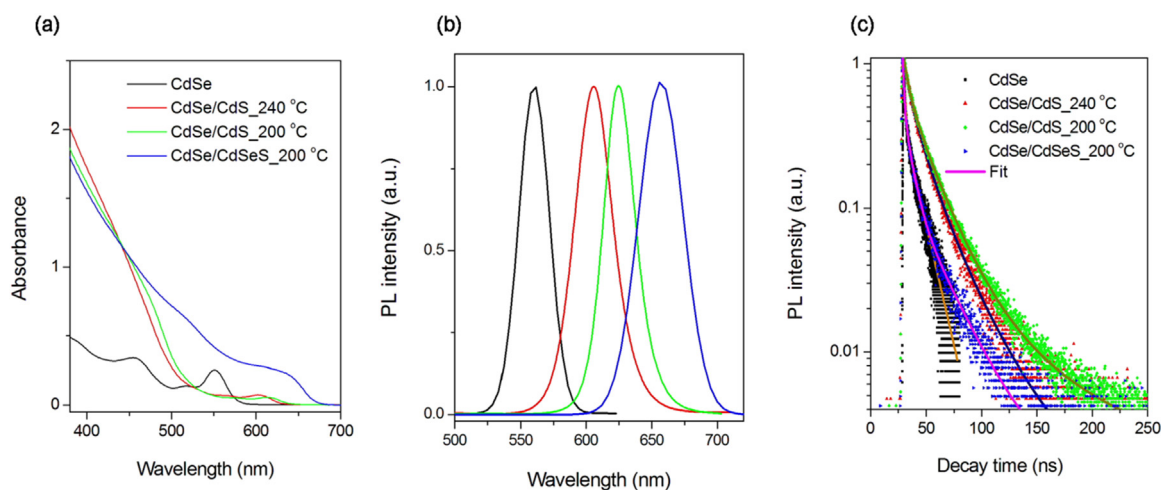


Fig. 2. Optical properties of QDs. Absorption (a) and PL (b) spectra of CdSe QDs before and after shell coating at different temperatures. (c) Typical PL decay curves (dots) and fitting curves (solid lines) for CdSe, CdSe/CdS and CdSe/CdSeS QDs with different reaction temperatures measured at the emission peak in toluene, shown on a semi-logarithmic scale. The excitation wavelength was set at 450 nm.

Table 1

Structure and optical properties of the colloidal QDs with different morphologies.

QDs	Morphology	Core radius (nm)	Overall diameter (nm)	QY (%)	τ_{meas} (ns)	τ_{rad} (ns)	k_{rad} (ns^{-1})	k_{nr} (ns^{-1})
CdSe	spherical	1.65	3.3	20 ± 2	10 ± 1	50	0.02	0.08
CdSe/6CdS	spherical	1.65	7.2 ± 0.5	50 ± 4	25 ± 1	50	0.02	0.02
CdSe/6CdS	pyramidal	1.65	8 ± 0.6	40 ± 4	30 ± 1	75	0.013	0.02
CdSe/5CdSe _{0.5} S _{0.5} /CdS	pyramidal	1.65	8.1 ± 0.7	15 ± 2	15 ± 1	100	0.01	0.06

of 500–600 nm is very weak (Fig. 2a) [22,37,44,45]. Compared with spherical shape CdSe/CdS QDs (240 °C), the pyramidal CdSe/CdS QDs (200 °C) exhibit a red-shift of ~20 nm for both first-excitonic absorption and emission peak due to the electron leakage (Fig. 2a,b and Fig. S8). With further addition of Se in the CdS shell, the alloyed CdSe_{0.5}S_{0.5} shell expands the absorption of pyramidal QDs from 500 nm to 670 nm, matching very well with the Sun's spectrum in the visible range, indicating that the alloyed thick-shell QDs could be an excellent candidate as light absorbers for optoelectronic devices (Fig. 2a,b). Similar alloyed core/shell system has been reported previously for spherical CdSe/Cd_xPb_{1-x}S QDs [38] and CdSe/CdSe_xS_{1-x}/CdS QDs [14,41]. The typical quantum yields (QYs) of CdSe, spherical CdSe/CdS, pyramidal CdSe/CdS and CdSe/CdSe_{0.5}S_{0.5}/CdS in toluene are 20%, 50%, 40% and 15%, respectively (Table 1). Usually, higher QY in QDs indicates that the QDs have a better surface passivation with less surface recombination centers [35,46]. In order to understand the nature of QY in different morphologies of QDs, we measured the photoluminescence (PL) lifetime of QDs (Table 1). The radiative decay rate (k_{rad}) and the non-radiative decay rate (k_{nr}) in QDs were estimated according to the following equations: [47]

$$QY = \frac{\tau_{\text{meas}}}{\tau_{\text{rad}}} QY = \frac{\tau_{\text{meas}}}{\tau_{\text{rad}}} = \frac{k_{\text{rad}}}{k_{\text{nr}} + k_{\text{rad}}} \quad (1)$$

where τ_{meas} , τ_{rad} and τ_{nr} are the measured PL lifetime and the radiative lifetimes respectively. The calculated k_{rad} and k_{nr} are shown in Table 1.

For the CdSe QDs, k_{nr} is ~0.08 ns^{-1} , while for the spherical or pyramidal CdSe/6CdS QDs, k_{nr} decreases to ~0.02 ns^{-1} . In the pyramidal alloyed-shell CdSe/5CdSe_{0.5}S_{0.5}/CdS QDs, k_{nr} is ~0.06 ns^{-1} . As the non-radiative decay rate (k_{nr}) is mainly induced by the surface chemical states (e.g. surface defects and traps, quenchers), [25,46,47] the higher k_{nr} in CdSe or CdSe/5CdSe_{0.5}S_{0.5}/CdS QDs proves that these QDs are more sensitive to the surrounding surface chemical states and there may be more surface defects/traps on bare CdSe QDs and alloyed-shell QDs compared with core/thick-shell CdSe/CdS QDs. Generally, k_{r}

is depending on the size, shape, and heterostructure of QDs [15,16,27]. As reported in the literature, in the core/shell system, the spherical PbSe/CdSe/CdS QDs have a much longer radiative lifetime compared with PbSe/CdSe QDs [27]. Similarly, the radiative lifetime in pyramidal CdSe/CdS (or CdSe/CdSe_{0.5}S_{0.5}) core/thick-shell QDs is more than 1.5 times (or 2 times) longer than that in spherical CdSe/CdS QDs (Table 1), indicating the strong electron leakage in the pyramidal core/shell QDs [27,34]. In the plain QDs, the e/h wavefunction can spread over the entire QDs and easily reaches the surface of QDs, being quenched by the surrounding ligands/solvent, or suffering recombination due to the surface defects/traps [19,48]. These effects lead to the low QY in bare QDs. In the core/shell QDs, depending on the electronic band structure of the core/shell materials, the e/h can be either confined in the core or partially leaking into the shell, leading to a high QY in these systems (type I or quasi-type II) [19,21,27,34–37,48]. Typically, in the type II structure (both electron and hole can still spread into the entire shell region) the e/h still can spread at the surface of QDs, which is sensitive to the surface defects/traps and surrounding chemical conditions, leading to the low QY, similar to the bare QDs system [48]. This may explain the low QY in the bare CdSe and CdSe/5CdSe_{0.5}S_{0.5}/CdS and high QY in CdSe/CdS QDs. To prove our hypothesis, we produced the sample CdSe/5CdSe_{0.5}S_{0.5}, in which we did not cap the QD with a protective CdS shell. Under these conditions, we expect a strong contribution to surface defects/trap states in lowering the QY of the sample. The as-synthesized CdSe/5CdSe_{0.5}S_{0.5} QDs without a CdS shell have the QY of only 10%. With a further one-monolayer CdS coating, the QY increases to 15% due to the possible isolation between the alloyed shell and surrounding chemical conditions. In this study, we only focus on the thick-shell QDs with five monolayers of CdSe_{0.5}S_{0.5} and one monolayer of CdS.

As the efficient charge transfer of QDs to e/h scavengers not only depends on surface recombination number but also largely relies on radiative lifetime [7,13]. To further understand the expected exciton dynamics in pyramidal core/shell QDs, the electron [ψ_e] and hole [ψ_h] wavefunctions of spherical and pyramidal QDs were calculated by

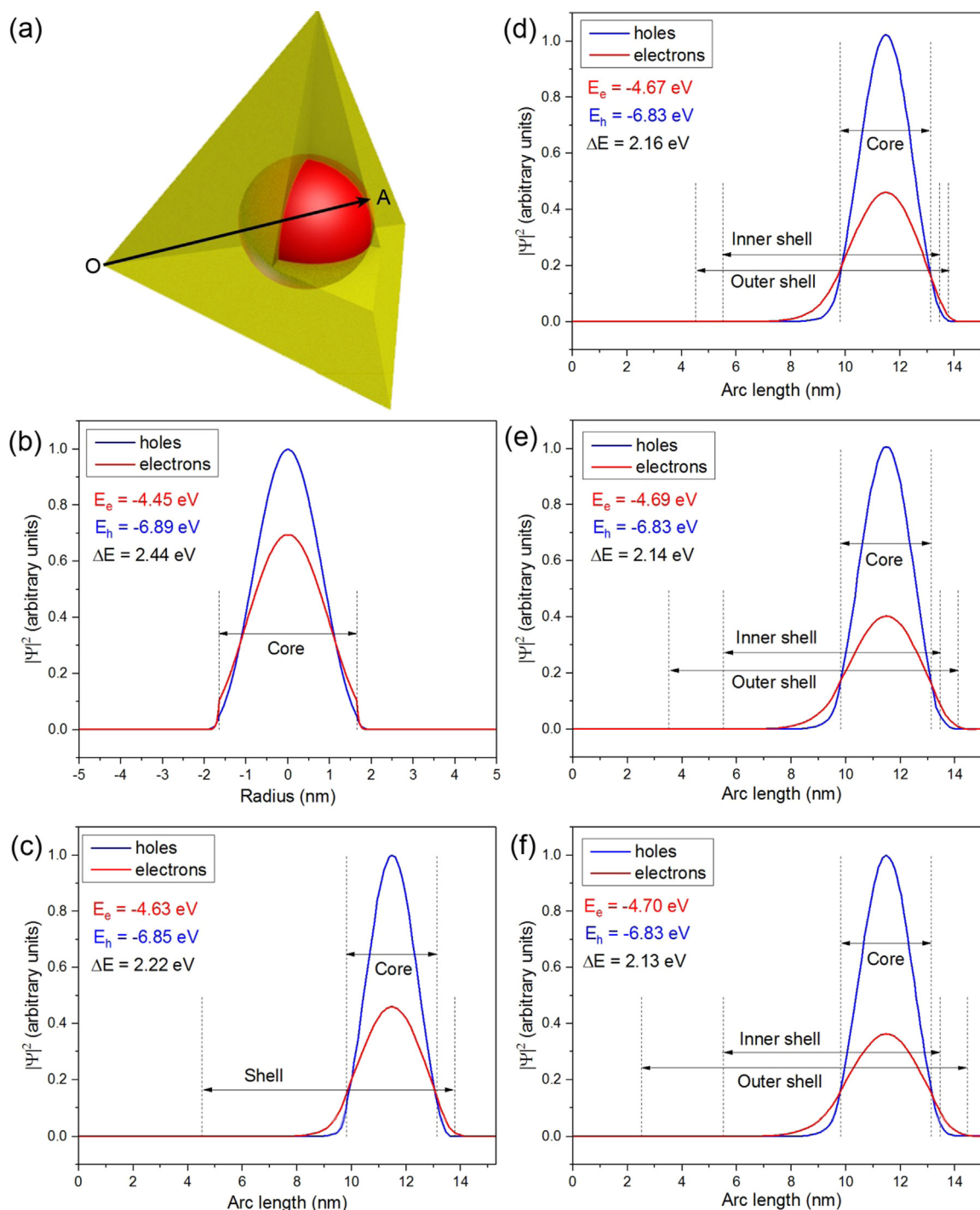


Fig. 3. Theoretical modeling of the CdSe/CdS and CdSe/CdSeS/CdS QDs. (a) Geometrical model of a pyramidal core/shell QD. The spherical CdSe core is in the center of the pyramidal QD. (b–f) Wavefunctions of 1S electrons and holes in the spherical CdSe QD along an axis passing through the center of the core (b), pyramidal CdSe/CdS QD (c), and pyramidal CdSe/CdSeS/CdS QDs with different CdS thicknesses (d–f). The arc length is defined as the distance from one corner of the pyramid to the opposite face (O→A in (a), passing through the center of the core). The CdSe core radius is 1.65 nm. The CdS shell thickness in (c) from the surface of the core to A is 0.66 nm while the corresponding thickness of the CdSeS layer is 0.33 nm in (d–f). The CdS shell thicknesses are 0.33, 0.66 and 1.00 nm in (d), (e) and (f), respectively. The eigenvalues for the electron and hole wave functions are given as E_e and E_h , respectively, while $\Delta E = E_e - E_h$. The general trend in ΔE is consistent with Fig. 2b.

solving the stationary Schrödinger wave equation in spherical or pyramidal geometry (Fig. 3). Compared to the symmetric distribution of e/h wavefunction of the spherical QDs, the e/h wavefunction of pyramidal core/shell QDs have an asymmetric e/h distribution. As shown in Fig. 3c–f, both the electron and hole wavefunctions leak more to the corner of pyramidal QDs (center of QD to O direction) than to the face center of pyramidal QDs (center of QD to A direction), presenting an

enhanced spatial separation of e/h in the QDs. The pyramidal QDs with an alloyed layer (Fig. 3d–f) have more e/h leakage with respect to that in pure-shell pyramidal QDs (Fig. 3c) due to the smoother transition from the core to the alloyed layer. In the alloyed pyramidal CdSe/CdSeS/CdS QDs with the constant thickness of CdSeS layer, the electron wavefunction does not exhibit strong changes with the increase of CdS thickness (from 0.33 nm to 1 nm) (Fig. 3d–f). The e/h wavefunctions are

still confined mainly in the core and interfacial shell region. These results are consistent with the long radiative lifetime in pyramidal QDs compared with spherical CdSe/6CdS QDs, even the QY in these QDs is not so high compared to the spherical CdSe/CdS QDs. The shape-dependent e/h wavefunction indicates that the pyramidal QDs can be good candidates for optoelectronic devices benefiting from their efficient charge separation.

2.3. PEC devices for H₂ production

Compared with the spherical shape CdSe/CdS QDs, the e/h wave functions of the asymmetric QDs have a larger spatial extension due to spreading toward the corners of QDs. This feature is associated with very promising properties as light absorbers for optoelectronic devices because the long lifetime can improve the charge transfer rate with respect to the fast e/h recombination, such as PEC water splitting and QDs sensitized solar cells. As a proof-of-concept, the as-prepared CdSe/6CdS and CdSe/5CdSe_{0.5}S_{0.5}/CdS core/shell QDs were deposited into a mesoporous TiO₂ film to prepare the QDs-TiO₂ hybrid photoanodes for PEC H₂ generation. The thickness of the photoanodes (TiO₂/QDs/ZnS) is estimated to be around 14.3 μm based on the cross-sectional SEM image (Fig. S9). We evaluated the performance of PEC devices using a standard three-electrode configuration, [7] consisting of a QDs-TiO₂ working electrode, a Pt counter electrode, and a KCl saturated Ag/AgCl reference electrode, which is most used PEC configuration so far for QDs based PEC devices. [7,49,50] Hole scavengers (SO₃²⁻/S²⁻) were used as the electrolyte in order to improve the hole transfer rate. [7,13] The calculated band energy levels of QDs are presented in Fig. 4, which is favorable for not only charge transfer from QDs to TiO₂, but also for the reduction and oxidation energy levels of water. Generally, after sunlight illumination, the photogenerated electrons injected from QDs into the TiO₂ and then transferred to the front electrode, finally flew to the Pt counter electrode to participate in the reduction reaction of water for H₂ generation (Fig. 4). On the other side, the photogenerated holes react with SO₃²⁻/S²⁻, instead of the water due to the higher energy level of SO₃²⁻/S²⁻ compared with the oxidation potential of water. In fact, in this configuration with the presence of hole scavengers, only H₂ can be produced, other than H₂ and O₂ through water splitting. [7]

In order to fairly compare the properties of QDs with different morphologies, we fabricated all PEC devices using different types of QDs under identical sample preparation and measurement conditions. The performance of PEC cells based on QDs/TiO₂ anode is shown in Fig. 5a. The *J* (0.6 V vs RHE) is obtained as ~7.0 mA/cm² for the spherical CdSe/6CdS QDs, which is much higher than the value (~5.0 mA/cm²) of the bare CdSe QDs. As the *J* is only 0.3 mA/cm² for the photoanode based on bare TiO₂ (Fig. S10), the higher *J* of the QD-based anode is mainly attributed to the contribution of QDs. The *J* further increases to 8.3 mA/cm² for the pyramidal CdSe/6CdS QDs. The

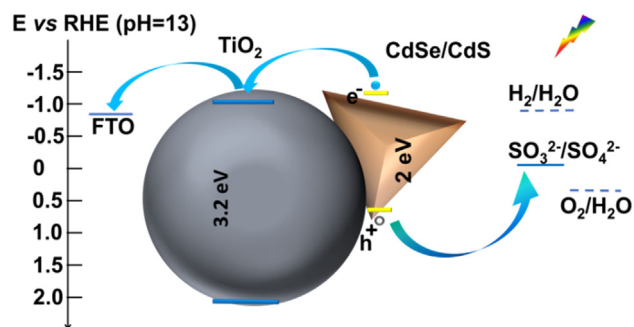


Fig. 4. Schematic electronic band structure of QDs. Schematic diagram and approximate band alignment of CdSe/CdS QDs-sensitized TiO₂ photoanodes. The bandgap of pyramidal CdSe/6CdS QDs was calculated based on their first-excitonic absorption peak.

18% enhancement in *J* of pyramidal CdSe/CdS QDs compared to spherical CdSe/CdS QDs is mainly due to the efficient e/h separation and transport as in both cases, the absorption spectrum of spherical or pyramidal CdSe/CdS QDs is similar (300–500 nm). In the case of PEC cell using pyramidal alloyed-thick-shell QDs/TiO₂ as the photoanode, the obtained *J* reaches 11.4 mA/cm² (0.6 V vs RHE), which is 1.4 times higher than that of the photoanode based on pyramidal CdSe/CdS QDs. This increase is mainly attributed to the wider absorption range in the core/alloyed-shell QDs as confirmed by the *J*-*V* measurement using an optical filter (Fig. S11). The saturated current density is as high as 12 mA/cm² at 0.9 V vs. RHE. The reported highest current density refers to the pristine electrode. This value is higher than the reported *J* of PEC devices based on semiconductors, such as 10 mA/cm² (thick-shell CdSe/13CdS QDs-TiO₂) [7], ~3 mA/cm² (thick-shell CuInSe/CuInS QDs-TiO₂), [51] NiOOH/FeOOH/carbon dots/BiVO₄ (5 mA/cm²) [52]. To the best of our knowledge, this is the highest value obtained so far for thick-shell colloidal QDs (or “giant” QDs) based PEC devices (Table S1). It is worth to mention, the PEC device based on TiO₂ sensitized with CdS/CdSe QDs or PbS/Mn-doped CdS QDs prepared via in-situ deposition exhibit *J* of 14.9 mA/cm² and 22.1 mA/cm², respectively. However, compared with the photoanode based on colloidal QDs, the in-situ deposition approach is time-consuming and the stability of the PEC device is not good [50,53]. For example, after only 5 min illuminating, the *J* decreases ~45% of its initial value [50].

The stability of the photoanodes was investigated under one sun illumination (100 mW/cm² AM 1.5G) in 0.25 M Na₂S and 0.35 M Na₂SO₃ (pH 13) aqueous solution. The *J* vs. time evolution of the PEC system at 0.6 V vs. RHE is shown in Fig. 5d. One can see a 33% drop of the original current density after 3600 s in the PEC device based on CdSe/5CdSe_{0.5}S_{0.5}/CdS QDs (Table 2), which is comparable to that of the best previously reported photoanodes [7,13,28,51]. It is still very challenging to obtain highly stable photoanodes based on QDs, due to the photocorrosion and accumulated hole-induced photooxidation [7,13,28,51]. Further research direction may focus on the improvement of the long-term stability by understanding the photo-induced degradation of QDs and the engineering of QDs architecture. Based on Fig. 5d, we calculated the H₂ generation rate (details in Supporting information, Fig. S12) using CdSe/CdS QDs as a reference [7]. The H₂ generation rate is ~40, 54, 60 and 90 mL cm⁻² day⁻¹ for the photoanode based on bare CdSe, spherical CdSe/CdS, truncated-pyramidal CdSe/CdS, and truncated-pyramidal CdSe/5CdSe_{0.5}S_{0.5}/CdS QDs, respectively (Table 2). The H₂ generation rate of pyramidal thick-alloy-shell QDs is higher than the other types of QDs and among the best of the previously reported H₂ generation rates. [7,28,51]

3. Conclusions and perspectives

In summary, we prepared pyramidal thick-shell CdSe/CdS and CdSe/CdSe_xS_{1-x} QDs by the combination of hot injection and SILAR approaches. The morphology of QDs can be controlled by simply changing the reaction temperature. The core/alloyed-shell QDs with pyramidal shape exhibit the QY of ~15%, with a radiative lifetime of 100 ns, which is much longer than that of spherical QDs, due to the efficient spatial separation of e/h wave function as confirmed by both lifetime measurements and theoretical simulations. The pyramidal thick-alloy-shell QDs/TiO₂-based photoanode exhibits a saturated photocurrent density of ~12 mA/cm² (90 mL cm⁻² day⁻¹), which is a record for thick-shell QD-based photoelectrodes in PEC H₂ generation. This result can be ascribed to both the enhanced light absorption in the region of 500–700 nm, induced by the presence of the CdSe in the thick shell, and by the effective e/h separation, owing to the delocalized e/h electronic states inside the pyramid structure. Thick-shell pyramidal QDs present a promising efficient light absorption for QD-based optoelectronic devices. Further research direction may focus on the development of other types of asymmetric thick-shell QDs, such as InP/CdSe_xS_{1-x}/CdS, Cu(Zn)InS/CdSe_xS_{1-x}/CdS, PbS/CdSe_xS_{1-x}/CdS and

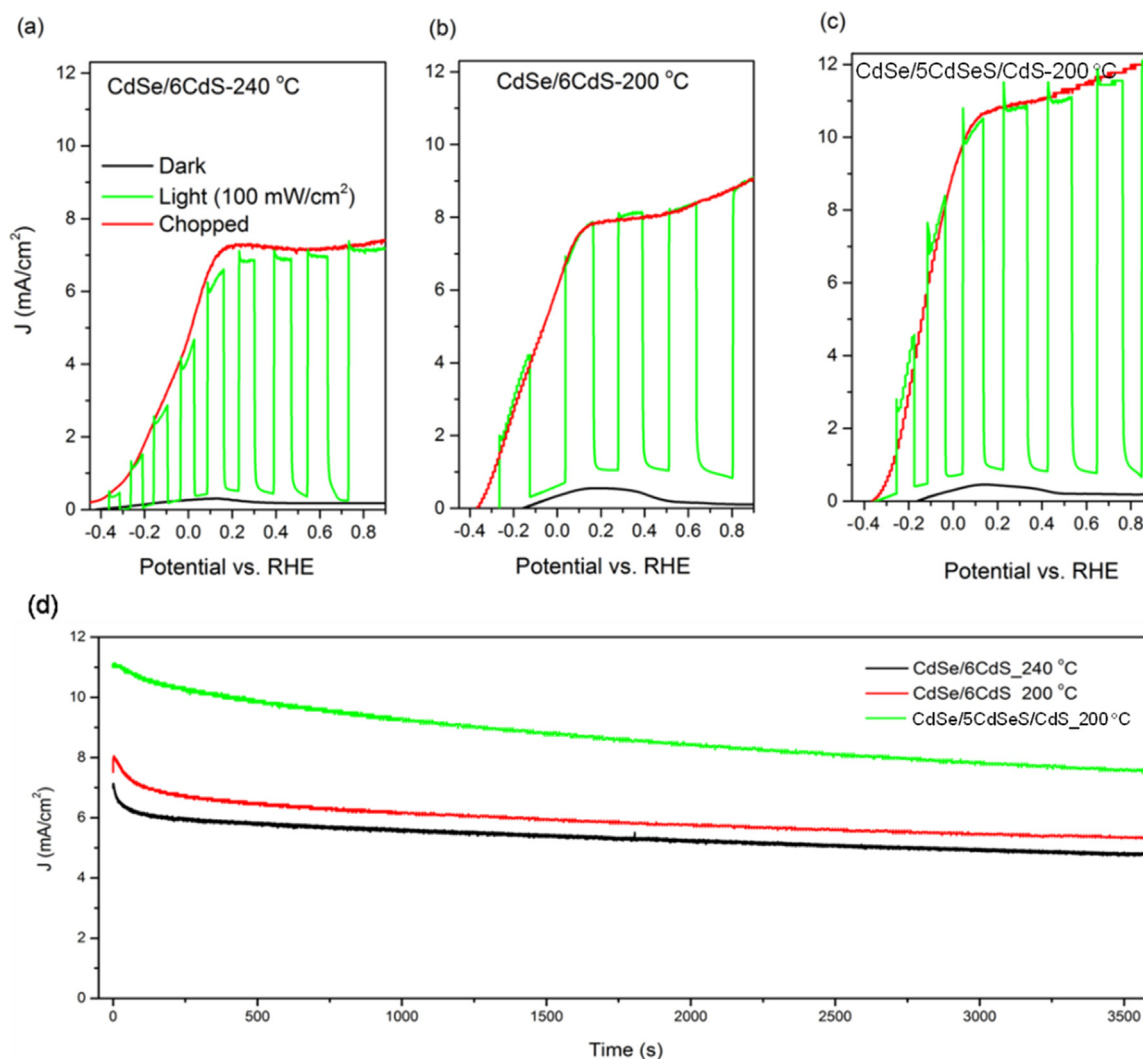


Fig. 5. Photogenerated current density. *J*-*V* dependence (versus RHE) of QDs-TiO₂-sensitized photoelectrodes in the dark (black curve), under continuous (red curve) and chopped (green curve) illumination (AM 1.5 G, 100 mW/cm²) of different kinds of QDs: (a) CdSe/6CdS synthesized at 240 °C; (b) pyramidal CdSe/6CdS QDs synthesized at 200 °C; (c) pyramidal alloyed CdSe/5CdSeS/CdS QDs synthesized at 200 °C. (d) Measured photocurrent density of QDs, with different QD morphologies, as a function of time at 0.6 V vs. RHE under simulated one sun illumination (100 mW/cm²).

Table 2

Performance of the PEC devices based on colloidal QDs.

QDs	Morphology	<i>J</i> (mA cm ⁻²)	<i>J</i> after one hour illumination (mA cm ⁻²)	H ₂ generation rate (mL cm ⁻² day ⁻¹)
CdSe	spherical	5.3	3.6	40
CdSe/6CdS	spherical	7.0	4.8	54
CdSe/6CdS	pyramidal	8.3	5.3	60
CdSe/ 5CdSe _{0.5} ⁻ S _{0.5} /CdS	pyramidal	11.4	7.6	90

PbSe/CdSe/CdS QDs.

4. Experimental section

4.1. Synthesis of thick-shell QDs

CdSe QDs were synthesized by using a hot injection method as described elsewhere [38]. Details were included in the Supporting information. The SILAR approach was used to grow spherical core/shell

QDs [21,27,38]. Similar with the procedure for the synthesis of spherical core/shell QDs (details in Supporting information), the SILAR approach was used to synthesize pyramidal core/shell QDs. In details, oleylamine (5 mL), octadecene (ODE) (5 mL) and CdSe QDs ($\sim 2 \times 10^{-7}$ mol in hexane) were degassed at 100 °C for 1 h. The reaction flask was re-stored with N₂ and the temperature was raised to 200 °C. The Cd(OA)₂ dispersed in ODE (0.25 mL, 0.2 M) was added dropwise and the mixture allowed to react for 1.5 h, followed by dropwise addition of 0.2 M S/ODE with 0.25 mL. The shell was further annealed for 10 min at 200 °C. All subsequent shells were annealed at 200 °C for ~ 10 min following the injection of S and ~ 1.5 h following addition of the Cd(OA)₂ in ODE. In the synthesis of thick-shell pyramidal CdSe/5CdSe_xS_{1-x}/CdS QDs, the reaction was conducted at 200 °C with the addition of five-monolayer S/Se and Cd(OA)₂ precursors and one-monolayer S and Cd(OA)₂ precursor. The reaction was cooled to 25 °C using ice water. Ethanol was added, then the suspension was centrifuged and the supernatant was removed. This purification procedure was repeated twice. The QDs were then dispersed in a solvent (e.g. toluene, hexane).

4.2. Preparation of QDs/TiO₂ photoanode

The hybrid anode was prepared by deposition of QDs into mesoporous TiO₂ film by electrophoretic deposition (EPD). In detail, a thin and compact TiO₂ layer was spin-coated on cleaned FTO glass substrate at 5000 r.p.m. for 30 s by using the solution Ti-Nanoxide BL/SC, followed by annealing in air at 500 °C for 30 min, then cooled down to room temperature. Subsequently, a commercial TiO₂ paste made of a blend of small anatase particles (~20 nm in diameter) and larger anatase particles (up to 450 nm in diameter) paste was deposited on top of the compact TiO₂ layer by tape casting and dried in air for 15 min. The photoanodes were then fired on a hot plate at 120 °C for 6 min. The photoanodes were finally sintered at 500 °C for 30 min. Two as prepared TiO₂ films on FTO substrate were vertically immersed in the QDs toluene solution. The distance between them was adjusted at 1 cm and a direct current bias of 200 V was applied for 120 min. To wash off unbound QDs after the EPD process, the samples were rinsed three times with toluene and dried with N₂ at room temperature. Subsequently, for the ligand exchange, QDs/TiO₂ film is dipped in 20 mL CTAB/methanol solution (10 mg/mL) for 1 min. Then the photoanode is rinsed with methanol for 1 min. Then the ZnS capping layer was formed by the SILAR process. Two SILAR cycles were applied to form the capping ZnS layer.

4.3. Theoretical calculation of *e/h* wave functions

We solved the stationary Schrödinger equation in spherical and pyramidal geometry by following the methodology reported in reference [14]. Detailed parameters are included in the [Supporting information](#).

4.4. Characterizations

TEM was carried out using a JEOL 2100F TEM equipped with a SAED and an EDS. XPS was performed on a VG Escalab 220i-XL equipped with hemispherical analyzer recorded for a Twin Anode X-Ray Source. Absorption spectra were acquired with a UV-2600 UV-vis spectrophotometer (Shimadzu). Fluorescence spectra were acquired with a FLS980 (Edinburgh). The PL lifetimes of core/shell QDs were measured using a pulsed laser diode of 440 nm and time-correlated single photon counting (TCSPC) mode in the FLS980 system. Photoluminescence QYs of QDs was measured by using Rhodamine 6G as a reference.

4.5. PEC measurements

PEC performance of the photoelectrodes fabricated using spherical and pyramidal shaped QDs were measured in a three-electrode configuration. [28] Details were included in the [Supporting information](#). Briefly, the Pt was used as the counter electrode, QDs/TiO₂/FTO hybrid was used as photoanode and Ag/AgCl was used as reference electrode. Na₂S/Na₂SO₃ was used as (pH = 13, 0.25 M Na₂S and 0.35 M Na₂SO₃). The photoresponse was measured using an Oriel LCS-100 solar simulator (AM1.5G) with or without long-pass optical filter (600 nm and 500 nm) with the light impinging on the QDs/TiO₂ side of the substrate. The light intensity measured by power meter was ~100 mW/cm². The working area of the photoanode was ~0.1–0.2 cm². Current density as a function of time was measured at 0.6 V vs. RHE under continues AM 1.5G illumination. H₂ evolution was measured during the PEC experiment. The produced H₂ gas was detected using a Shimadzu GC-8A gas chromatograph (GC) equipped with a thermal conductivity detector. [7] Argon was used as the carrier gas for GC analysis. Based on the reference curve (Fig. S12), we integrate the current density (Fig. 5d), and the calculated hydrogen generation rate is illuminated in Table 2.

Acknowledgements

H.G. Zhao acknowledges the start fund from Qingdao University and the funding from the Natural Science Foundation of Shandong Province (ZR2018MB001). A. Vomiero acknowledges Knut & Alice Wallenberg Foundation, the Swedish Foundations Consolidator Fellowship, LTU Lab fund program and Kempe Foundation for partial funding, and the European Union's Horizon 2020 research and innovation programme under grant agreement No 654002. Y. Q. Wang would like to thank the financial support from the Recruitment Program of High-end Foreign Experts (Grant Nos.: GDW20163500110 and GDW20173500154), Taishan Scholar Program of Shandong Province, China, Qingdao International Center for Semiconductor Photoelectric Nanomaterials, and Shandong Provincial University Key Laboratory of Optoelectrical Material Physics and Devices.

Appendix A. Supporting information

Supplementary data associated with this article can be found in the online version at doi:10.1016/j.nanoen.2018.08.042.

References

- [1] H. Zhao, F. Rosei, *Chem* 3 (2) (2017) 229–258.
- [2] F. Navarro-Pardo, H. Zhao, Z.M. Wang, F. Rosei, *Acc. Chem. Res.* 51 (3) (2017) 609–618.
- [3] T. Hisatomi, J. Kubota, K. Domen, *Chem. Soc. Rev.* 43 (22) (2014) 7520–7535.
- [4] O. Khaselev, J.A. Turner, *Science* 280 (5362) (1998) 425–427.
- [5] G.M. Wang, H.Y. Wang, Y.C. Ling, Y.C. Tang, X.Y. Yang, R.C. Fitzmorris, C.C. Wang, J.Z. Zhang, Y. Li, *Nano Lett.* 11 (7) (2011) 3026–3033.
- [6] J. Qi, W. Zhang, R. Cao, *Adv. Energy Mater.* 8 (5) (2018) 1701620.
- [7] R. Adhikari, L. Jin, F. Navarro-Pardo, D. Benetti, B. Alotaibi, S. Vanka, H. Zhao, Z. Mi, A. Vomiero, F. Rosei, *Nano Energy* 27 (2016) 265–274.
- [8] X. Chen, L. Liu, P.Y. Yu, S.S. Mao, *Science* 331 (6018) (2011) 746–750.
- [9] A. Sasinska, T. Singh, S.Z. Wang, S. Mathur, R. Kraehnert, *J. Vac. Sci. Technol. A* 33 (1) (2015) 01A152.
- [10] T. Singh, T. Lehnen, T. Leuning, S. Mathur, Atomic layer deposition grown MOx thin films for solar water splitting: prospects and challenges, *J. Vac. Sci. Technol. A* 33 (1) (2015) 010801.
- [11] T. Singh, R. Mueller, J. Singh, S. Mathur, *Appl. Surf. Sci.* 347 (2015) 448–453.
- [12] Z. Wang, C. Yang, T. Lin, H. Yin, P. Chen, D. Wan, F. Xu, F. Huang, J. Lin, X. Xie, M. Jiang, *Adv. Funct. Mater.* 23 (43) (2013) 5444–5450.
- [13] L. Jin, G. Sirigu, X. Tong, A. Camellini, A. Parisini, G. Nicotra, C. Spinella, H. Zhao, S. Sun, V. Morandi, M. Zavelani-Rossi, F. Rosei, A. Vomiero, *Nano Energy* 30 (2016) 531–541.
- [14] G.S. Selopal, H. Zhao, X. Tong, D. Benetti, F. Navarro-Pardo, Y. Zhou, D. Barba, F. Vidal, Z.M. Wang, F. Rosei, *Adv. Funct. Mater.* 27 (30) (2017) 1701468.
- [15] A.P. Alivisatos, *Science* 271 (5251) (1996) 933–937.
- [16] W.E. Buhro, V.L. Colvin, *Nat. Mater.* 2 (3) (2003) 138–139.
- [17] C. Dang, J. Lee, C. Breen, J.S. Steckel, S. Coe-Sullivan, A. Nurmikko, *Nat. Nanotechnol.* 7 (5) (2012) 335–339.
- [18] O. Chen, H. Wei, A. Maurice, M. Bawendi, P. Reiss, *MRS Bull.* 38 (9) (2013) 696–702.
- [19] I. Coropceanu, M.G. Bawendi, *Nano Lett.* 14 (7) (2014) 4097–4101.
- [20] H. McDaniel, A.Y. Kopysov, S. Draguta, N.S. Makarov, J.M. Pietryga, V.I. Klimov, *J. Phys. Chem. C* 118 (30) (2014) 16987–16994.
- [21] Y. Chen, J. Vela, H. Htoon, J.L. Casson, D.J. Werder, D.A. Bussian, V.I. Klimov, J.A. Hollingsworth, *J. Am. Chem. Soc.* 130 (15) (2008) 5026–5027.
- [22] B. Mahler, N. Lequeux, B. Dubertret, *J. Am. Chem. Soc.* 132 (3) (2010) 953–959.
- [23] O. Chen, Y. Yang, T. Wang, H. Wu, C. Niu, J. Yang, Y.C. Cao, *J. Am. Chem. Soc.* 133 (43) (2011) 17504–17512.
- [24] W.K. Bae, Y.-S. Park, J. Lim, D. Lee, L.A. Padilha, H. McDaniel, I. Robel, C. Lee, J.M. Pietryga, V.I. Klimov, *Nat. Commun.* 4 (2013) 2661.
- [25] O. Chen, Y. Zhao, V.P. Chauhan, J. Cui, C. Wong, D.K. Harris, H. Wei, H.-S. Han, D. Fukumura, R.K. Jain, M.G. Bawendi, *Nat. Mater.* 12 (5) (2013) 445–451.
- [26] C.M. Cirloganu, L.A. Padilha, Q. Lin, N.S. Makarov, K.A. Velizhanin, H. Luo, I. Robel, J.M. Pietryga, V.I. Klimov, *Nat. Commun.* 5 (2014) 4148.
- [27] C.J. Hanson, N.F. Hartmann, A. Singh, X. Ma, W.J.L. DeBenedetti, J.L. Casson, J.K. Grey, Y.J. Chabal, A.V. Malko, M. Sykora, A. Piryatinski, H. Htoon, J.A. Hollingsworth, *J. Am. Chem. Soc.* 139 (32) (2017) 11081–11088.
- [28] L. Jin, B. Alotaibi, D. Benetti, S. Li, H. Zhao, Z. Mi, A. Vomiero, F. Rosei, *Adv. Sci.* 3 (3) (2016) 1500345.
- [29] X. Tong, Y. Zhou, L. Jin, K. Basu, R. Adhikari, G.S. Selopal, X. Tong, H. Zhao, S. Sun, A. Vomiero, Z.M. Wang, F. Rosei, *Nano Energy* 31 (2017) 441–449.
- [30] O. Chen, X. Chen, Y. Yang, J. Lynch, H. Wu, J. Zhuang, Y.C. Cao, *Angew. Chem. Int. Ed.* 47 (45) (2008) 8638–8641.
- [31] E. Cassette, B. Mahler, J.-M. Guigner, G. Patriarche, B. Dubertret, T. Pons, *ACS Nano* 6 (8) (2012) 6741–6750.
- [32] C. Pak, J.Y. Woo, K. Lee, W.D. Kim, Y. Yoo, D.C. Lee, *J. Phys. Chem. C* 116 (48)

- (2012) 25407–25414.
- [33] R. Tan, Y. Yuan, Y. Nagaoka, D. Eggert, X. Wang, S. Thota, P. Guo, H. Yang, J. Zhao, O. Chen, *Chem. Mater.* 29 (9) (2017) 4097–4108.
- [34] H. Zang, H. Li, N.S. Makarov, K.A. Velizhanin, K. Wu, Y.-S. Park, V.I. Klimov, *Nano Lett.* 17 (3) (2017) 1787–1795.
- [35] J. Zhou, M. Zhu, R. Meng, H. Qin, X. Peng, *J. Am. Chem. Soc.* 139 (46) (2017) 16556–16567.
- [36] G. Raino, T. Stoeferle, I. Moreels, R. Gomes, J.S. Kamal, Z. Hens, R.F. Mahrt, *ACS Nano* 5 (5) (2011) 4031–4036.
- [37] M. Cirillo, T. Aubert, R. Gomes, R. Van Deun, P. Emplit, A. Biermann, H. Lange, C. Thomsen, E. Brainis, Z. Hens, *Chem. Mater.* 26 (2) (2014) 1154–1160.
- [38] H. Zhao, D. Benetti, L. Jin, Y. Zhou, F. Rosei, A. Vomiero, *Small* 12 (38) (2016) 5354–5365.
- [39] Y. Ghosh, B.D. Mangum, J.L. Casson, D.J. Williams, H. Htoon, J.A. Hollingsworth, *J. Am. Chem. Soc.* 134 (23) (2012) 9634–9643.
- [40] J. Zhou, C. Pu, T. Jiao, X. Hou, X. Peng, *J. Am. Chem. Soc.* 138 (20) (2016) 6475–6483.
- [41] W.K. Bae, L.A. Padilha, Y.-S. Park, H. McDaniel, I. Robel, J.M. Pietryga, V.I. Klimov, *ACS Nano* 7 (4) (2013) 3411–3419.
- [42] K.P. Acharya, H.M. Nguyen, M. Paulite, A. Piryatinski, J. Zhang, J.L. Casson, H. Xu, H. Htoon, J.A. Hollingsworth, *J. Am. Chem. Soc.* 137 (11) (2015) 3755–3758.
- [43] S. Ghosh, R. Gaspari, G. Bertoni, M.C. Spadaro, M. Prato, S. Turner, A. Cavalli, L. Manna, R. Brescia, *ACS Nano* 9 (8) (2015) 8537–8546.
- [44] E. Bladt, R.J.A. van Dijk-Moes, J. Peters, F. Montanarella, Cd.M. Donega, D. Vanmaekelbergh, S. Bals, *J. Am. Chem. Soc.* 138 (43) (2016) 14288–14293.
- [45] W. Nan, Y. Niu, H. Qin, F. Cui, Y. Yang, R. Lai, W. Lin, X. Peng, *J. Am. Chem. Soc.* 134 (48) (2012) 19685–19693.
- [46] F. Ren, S.A. Lindley, H. Zhao, L. Tan, B.A. Gonfa, Y.-C. Pu, F. Yang, X. Liu, F. Vidal, J.Z. Zhang, F. Vetrone, D. Ma, *Phys. Chem. Chem. Phys.* 18 (46) (2016) 31828–31835.
- [47] Y. Zhou, D. Benetti, Z. Fan, H. Zhao, D. Ma, A.O. Govorov, A. Vomiero, F. Rosei, *Adv. Energy Mater.* 6 (11) (2016) 1501913.
- [48] S.A. Ivanov, A. Piryatinski, J. Nanda, S. Tretiak, K.R. Zavadil, W.O. Wallace, D. Werder, V.I. Klimov, *J. Am. Chem. Soc.* 129 (38) (2007) 11708–11719.
- [49] X.L. Zheng, J.P. Song, T. Ling, Z.P. Hu, P.-F. Yin, K. Davey, X.W. Du, S.Z. Qiao, *Adv. Mater.* 28 (24) (2016) 4935–4942.
- [50] J.Y. Kim, Y.J. Jang, J. Park, J. Kim, J.S. Kang, D.Y. Chung, Y.E. Sung, C. Lee, J.S. Lee, M.J. Ko, *Appl. Catal. B-Environ.* 227 (2018) 409–417.
- [51] X. Tong, X.-T. Kong, Y. Zhou, F. Navarro-Pardo, G.S. Selopal, S. Sun, A.O. Govorov, H. Zhao, Z.M. Wang, F. Rosei, *Adv. Energy Mater.* 8 (2) (2018) 1701432.
- [52] K.H. Ye, Z.L. Wang, J.W. Gu, S. Xiao, Y.F. Yuan, Y. Zhu, Y.M. Zhang, W.J. Mai, S.H. Yang, *Energy Environ. Sci.* 10 (3) (2017) 772–779.
- [53] Y.-L. Lee, C.-F. Chi, S.-Y. Liao, *Chem. Mater.* 22 (3) (2010) 922–927.



Guiju Liu received her Bachelor degree in Materials Physics from Qingdao University (China) in 2014. She obtained Master degree at Qingdao University (China) in 2017. Currently, she is a Ph.D. student majoring in Materials Physics and Chemistry at Qingdao University. Her research mainly focuses on the synthesis and structural characterization of quantum dots and their applications in luminescent solar concentrators and hydrogen generation.



François Vidal works on the theory and numerical modeling of various physical phenomena. After obtaining a Ph.D. from the University of Montreal (Canada) in Subatomic Physics, he worked as a research associate at CEA (France) and at INRS in the field of plasma physics. He then became a professor at INRS in 2003. In the last few years, he has been interested in materials science, in particular on DFT modeling of multiferroic materials and catalysis phenomena.



Yiqian Wang received his Ph.D. degree in condensed matter physics from Institute of Physics, Chinese Academy of Sciences, China in 2001. Then he worked as a research fellow at INRS-EMT, Canada and Imperial College London, UK. He is currently a Professor at Qingdao University. His research interest includes the fabrication and characterization of perovskite functional materials, as well as exploitation of their potential applications.



Alberto Vomiero is a chair professor in Experimental Physics at the Division of Materials Science, Department of Engineering Sciences and Mathematics, Luleå University of Technology (LTU), Sweden since October 2014. His main interests are in the synthesis of composite nanomaterials for environmental applications, including solar cells, water splitting and photocatalysis, and he is leading at LTU a multidisciplinary group of Physicists, Chemists, Engineers and Materials Scientists. He is a former Marie Curie International Outgoing Fellow of the European Commission, Fellow of the Swedish Foundations, of the Royal Society of Chemistry (UK), and of several other Societies.



Haiguang Zhao is Professor of College of Physics & The State Key Laboratory, Qingdao University, Qingdao (Shandong), China. He received M.Sc. degree (2007) from Zhejiang University and Ph.D. degree (2012) from Institut National de la Recherche Scientifique (INRS), Quebec University. His research interests focus on the synthesis of low-dimensional semiconductor materials (including metal oxide, quantum dot, nanoplatelets and inorganic perovskite) for solar energy applications, such as solar cell, luminescent solar concentrator and solar-driven water splitting.